Convective mixing by internal waves in the Puerto Rico Trench

by Hans van Haren[1,2] and Louis Gostiaux[3]

ABSTRACT

A 2.4 km long deep-sea mooring was deployed for 14 months in the Puerto Rico Trench, the deepest part of the Atlantic Ocean. Below its top buoyancy package, the mooring line held a 200 m long string of high-resolution temperature sensors and a current meter. Over the instrumented range between 6,004 and 6,204 m, waters are very weakly stratified, with local buoyancy frequency equaling about 1.9 times the semidiurnal tidal frequency. Besides quiescent waters, the detailed observations show regular vertical turbulent overturning associated with periodic warming and driven by internal tidal and inertial waves. During such episodes, the 4-day and 200 m vertically averaged dissipation rate increases from approximately 10^{-11} up to 10^{-9} m^2 s^{-3}, and eddy diffusivity increases from 5 × 10^{-5} up to 4 × 10^{-3} m^2 s^{-1}. No large-scale shear-driven Kelvin-Helmholtz billows are observed, and free convection seems the dominant primary turbulent overturning mechanism affecting material redistribution and life in the weakly stratified environment.

Keywords: High-resolution temperature observations; Puerto Rico Trench; deep-ocean convection in weak stratification

1. Introduction

As the ocean is basically stably stratified in density from surface to bottom, vertical ("diapycnal") turbulent exchange is hampered (Gargett 1984), but not blocked. In fact, open oceans' weak vertical turbulent exchange is still 100-fold larger than molecular diffusion (Gregg 1989). In the strongly stratified portions of open seas and oceans away from boundaries, the main process behind diapycnal exchange is shear instability of (partially) opposing currents above and below the pycnocline in combination with (the sparse breaking of) high-frequency internal waves supported by the same stratification (e.g., Geyer and Smith 1987; Seim and Gregg 1994).

Although the stratification gradually decreases with increasing depth, completely homogeneous waters are rare. Nevertheless, turbulence characteristics are expected to change

1. Royal Netherlands Institute for Sea Research (NIOZ), P.O. Box 59, 1790 AB Den Burg, the Netherlands.
2. Corresponding author: *e-mail: hans.van.haren@nioz.nl*
3. Laboratoire de Mécanique des Fluides et d'Acoustique, UMR CNRS 5509, École Centrale de Lyon, Université de Lyon, 36 avenue Guy de Collongue, 69134 Écully cedex, France.
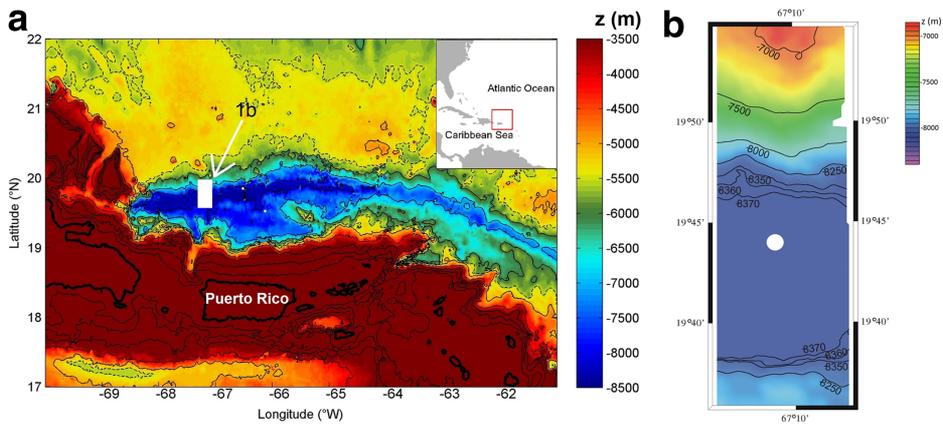
Figure 1. Area maps. (a) Puerto Rico Trench (PRT) bottom topography, using the 9.1 ETOPO-1 version of Smith and Sandwell (1997). Solid black contours every 1,000 m; the heavy (bold) contour denotes 0 m (land); the dashed contour is for 5,500 m, the approximate "top" of the PRT. (b) Detail area of panel (a), map from R/V *Pelagia*'s multibeam, with mooring and conductivity-temperature-depth site within the white dot. Note the different contouring (50 m) and color intervals, with respect to panel (a).

from mainly shear induced in strongly stratified waters to convection induced in near-homogeneous waters near the surface (e.g., Moum, Caldwell, and Paulson 1989) and in the deep ocean.

Here, we investigate in some detail the vertical exchange process in a deep-sea trench, which is not found to be a stagnant pool of cold water. It is dominated by internal tidal and large-scale subinertial eddy motions.

2. Data and handling

Moored observations have been made at the deepest part of the Puerto Rico Trench (PRT), Milwaukee Deep (Fig. 1). The mooring had a 200 m long thermistor string and a single Nortek AquaDopp acoustic current meter below its top buoyancy of 22 glass spheres, providing nearly 250 kg net buoyancy near 5,960 m below the surface. The current meter was equipped with pressure and tilt sensors. The mooring was deployed from the R/V *Pelagia* at 19°44′ N, 67°11′ W in 8,370 m water depth (measured using a Kongsberg-Simrad EM300 multibeam echosounder system calibrated with local conductivity-temperature-depth [CTD] data) on 11 December 2013 (year day 344). It was recovered on 10 February 2015 (year day 770). Several cross sections with the R/V *Pelagia*'s multibeam confirmed the flatness of the bottom deep, which had a width of 12 km in north–south direction (Fig. 1b). The mooring site was approximately 3 km from the foot of the northern slope.

The thermistor string consisted of 101 high-resolution, high-precision NIOZ4 temperature sensors (for characteristics, see van Haren et al. 2009). The sensors were spaced at 2.0

m intervals between 6,004 and 6,204 m and sampled at a rate of 1 Hz. They were synchro-
nized via induction every 4 h, so that timing mismatch was <0.02 s. Their noise level was
approximately 10^{-4} °C, about twice the standard level to accommodate for the long mooring
duration. Energy consumption is regulated by shortening the measurement time of the Wien
Bridge oscillator from the standard 0.1 to 0.05 s. Ten sensors, at positions (from the top of
the string) 3, 39, 53, 63, 67, 69, 85, 96, 97, and 99 failed and are not further considered.

The sensors were calibrated at the Royal Netherlands Institute for Sea Research (NIOZ)
using a 0.085 m^3 (∼85 L) thermostatic bath with preset temperature levels every 1°C
between −3°C and 30°C. Because sensors and SeaBird SBE35 reference thermometer
were held in a 0.03 m thick titanium bottom plate, temperature levels were kept constant
to within ±10^{-4}°C. To correct for the sensors' electronics drift of approximately 10^{-3}°C
per month after aging, vertical temperature profiles are considered, which are averaged
over a suitable length of time, typically 4–8 days, which exceeds, generally by a factor of
10, the largest turbulence overturning timescale and the longest internal wave period. In
such an average, with by nature turbulence and internal wave motions removed, a vertical
temperature profile should be smooth and at least be homogeneous, more commonly stably
stratified. This is achieved by fitting a polynomial, most commonly of third order, to the
average profile. For each sensor, all its temperature data within that particular 4- to 8-day
period are corrected with a single constant value to this smooth, statically stable profile.
This correction is repeated for other periods resulting in different corrections because of
the drift. The procedure is straightforward under typical ocean-stratification conditions, but
rather difficult under conditions where the stratification is weaker than the adiabatic lapse
rate (in an absolute sense). As this is the case in the present data, the electronics drift is
here, for each ∼6-day period, first corrected to a constant, homogeneous profile thereby
implicitly also compensating for the adiabatic lapse rate. Second, the data are transferred
to conservative (∼potential) temperature (Θ) values (Intergovernmental Oceanographic
Commission, Scientific Committee on Oceanic Research, and International Association for
the Physical Sciences of the Oceans 2010) by adding constant mean $\Theta(z)$, and thus $d\Theta/dz$,
values from local CTD observations.

For that purpose, approximately 1 km from the mooring, several shipborne SeaBird-911
CTD profiles were obtained, to a maximum depth of 7,200 m because of pressure sensor
and cable length constraints. The CTD data are also needed to establish the local density-
temperature relationship for use of the moored temperature sensor data as a tracer for
potential density anomaly variations, referenced to 6,000 m, σ_6. With such a relationship,
the number of NIOZ4 temperature sensors and their 2 m resolution are sufficient to use
these moored data to estimate turbulent flux parameters through the resolution of scales of
up to the largest energy-containing Ozmidov scales of turbulence in stratified fluids. Thus,
following Thorpe (1977) for CTD data and applied to moored temperature sensor data by
Levine and Boyd (2006) and van Haren and Gostiaux (2012), the turbulent kinetic energy
dissipation rate, $\varepsilon = C_0^2 d^2 N^3$, with $C_0 = 0.8$ a constant (Dillon 1982), and the vertical
(z) turbulent eddy diffusivity, $K_z = \Gamma \varepsilon N^{-2}$, with Γ the mixing efficiency coefficient,

are estimated by calculating "overturning displacement" scales d after reordering every (drift corrected) potential density (temperature) profile, which may contain inversions, into a stable monotonic profile without inversions (Thorpe 1977). N is computed from the reordered density (temperature) profiles. The estimate of ε (or, equivalently, the vertical heat flux) is relatively robust and can be made to within a factor of about 2 (van Haren and Gostiaux 2012). The indirect estimate of K_z is more problematic, as it depends on the mixing efficiency. Debate is ongoing, but the best option without further information to within an order of magnitude seems a constant value (e.g., Oakey 1982).

Thus, a constant, mean $\Gamma = 0.2$ is used, which is most commonly used under shear-induced, high–Reynolds number turbulent stratified-ocean conditions and yields $K_z = 0.128d^2N$ (Osborn 1980; Oakey 1982; Levine and Boyd 2006). Specifically here, a threshold of $\Delta T_{\text{thres}} = 2 \times 10^{-4}$ °C is used for accepting nonzero overturns. This threshold is half because of noise and half because of remaining temperature shifts after calibration (van Haren et al. 2009). In the following, averaging over depth range is indicated by $< \ldots >$, and over time by $[\ldots]$.

3. Observations

a. Yearlong overview

The location of the temperature sensors was approximately 500 m below the surrounding ocean floor, so near the top of the trench. Between 5,000 and 5,500 m, CTD profiles (Fig. 2) showed a transition from locally stronger stratification to weakly stratified waters. At the depth of the sensors, the stratification is dominated by temperature variations, but the gradient of the latter amounts to $d\Theta/dz = 3.5 \times 10^{-5}$°C m^{-1} (Fig. 2e). This value is only one-quarter of the local adiabatic lapse rate of 1.5×10^{-4}°C m^{-1}. Between 5,900 and 6,300 m, the linear temperature-density relationship is reasonably tight as $\delta\sigma_6 = \alpha\delta\Theta$, $\alpha = -0.185 \pm 0.005$ kg m^{-3}°C^{-1} (Fig. 2d). Repeated CTD observations show very little variation in this relationship, and the effects of salt-compensated intrusions are confirmed negligible. As a result, the temperature sensor observations can be used as a tracer for density variations to estimate turbulence parameters.

The mean buoyancy frequency over a scale of 100 m is $N_{100} = 2.6 \pm 1 \times 10^{-4}$ s$^{-1} = 1.9 \pm 0.8 f_h$, where $f_h = 2\Omega \cos\varphi$ denotes the horizontal Coriolis parameter of Earth rotational vector $\mathbf{\Omega}$ at latitude φ suggested to be important for delimiting convective exchange in weakly stratified waters (van Haren 2008). It is noted that in the PRT, $f_h = 0.98M_2$, where M_2 denotes the lunar semidiurnal tidal frequency. This N_{100} value is compared with spectral observations subsequently, as it associates with the upper limit of the internal wave band and thus a particular change in spectral slopes. The error in N_{100} value is commensurate with the uncertainty found in determining the buoyancy frequency in near-homogeneous waters (van Haren and Millot 2006). The locally strongest stratification of $N_{\max} = 6f_h$ is found at 5,300 m capping the PRT waters (Fig. 2a) and in occasional small-scale thin layers below.
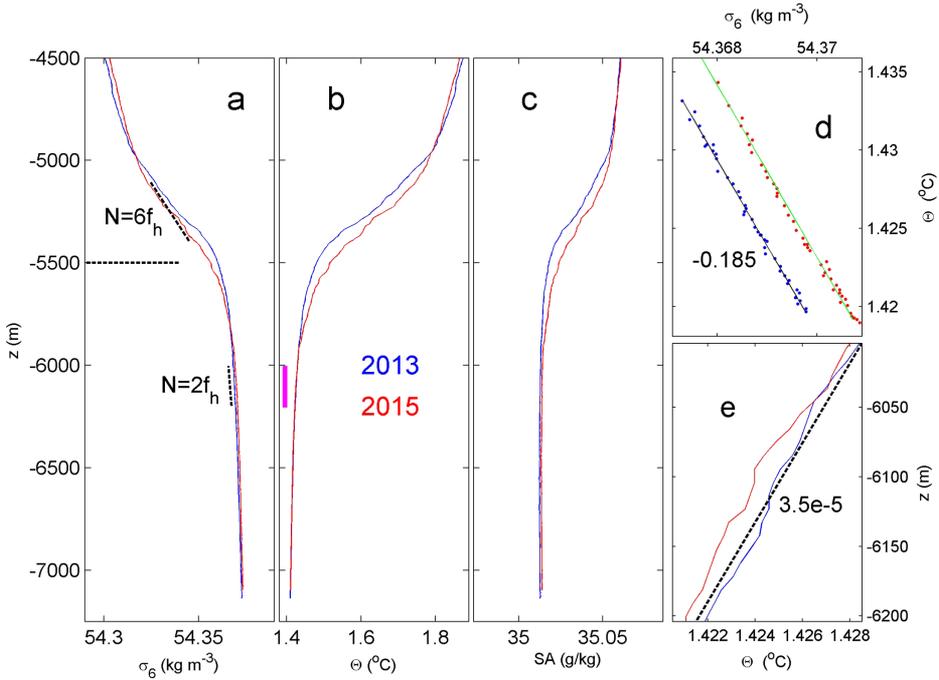
Figure 2. Overview of conductivity-temperature-depth data obtained at 1 km from the mooring site, during the deployment ("2013," blue) and recovery ("2015," red) cruises. (a) Potential density anomaly, referenced to 6,000 m. The indicated slope is for maximum buoyancy frequency $N_{max} = 6f_h$ (see text). The small dashed line indicates the approximate top of the Puerto Rico Trench. (b) Conservative temperature. The vertical bar indicates the range of the moored temperature measurements (purple). (c) Absolute salinity (SA). (d) Conservative temperature–density anomaly relationship for the vertical range of [5,900, 6,300] m. (e) Detail of panel (b), for the range of temperature sensors with the mean slope of $3.5 \times 10^{-5} °C\ m^{-1}$ indicated.

Overall, the temperature variations with time were dominated by large 20- to 40-day periodicities that modulated shorter timescale variations (Fig. 3a). No effects were noticed in the temperature observations from mooring deflections by current drag, despite the top of the mooring being lowered twice by 1.2 m because of implosion of three glass spheres or a loss of 75 kg of buoyancy and equivalent tension cable stretch at 3 and 26 days after deployment. With the remaining ~90 kg of net buoyancy, the mooring remained upright, and, because of the relatively low current speeds of <0.08 m s^{-1}, the top never deflected more than 2 m vertically as a result of drag. Only twice after day 371 did the top of the mooring sink more than 1 m (~1 dbar) vertically for the duration of a few days (Fig. 3b, around days 388 and 675 when currents were maximum; the current meter stopped recording after 11 months, the intended duration of deployment).
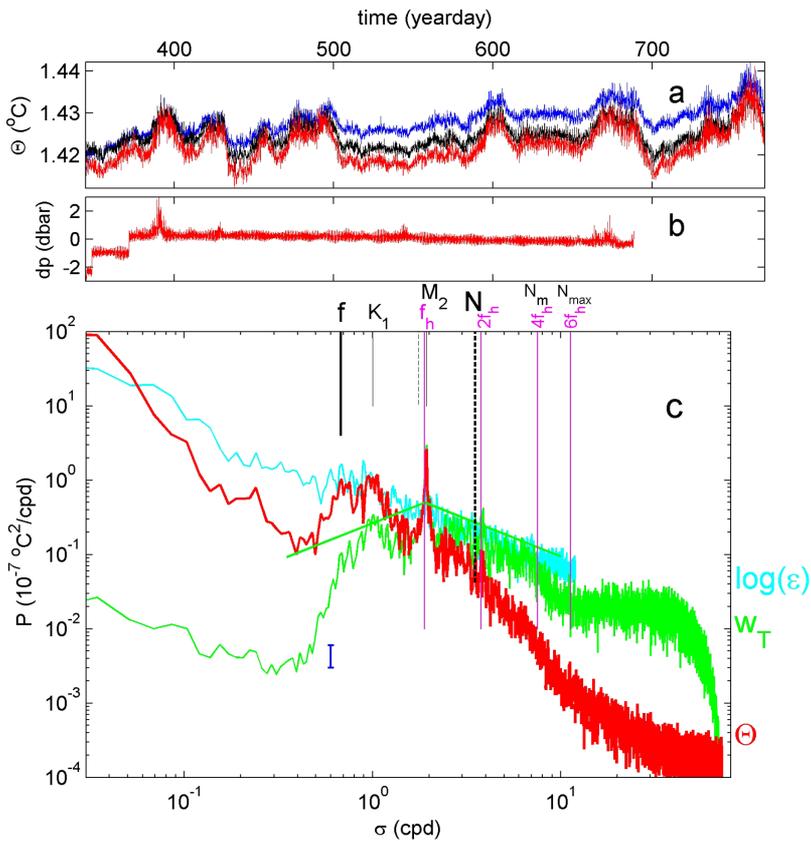
Figure 3. Overview of moored observations between 6,004 and 6,204 m in the upper level of the Puerto Rico Trench waters. (a) Entire 14 months of high-resolution conservative temperature time series (subsampled every 600 s, 10 min) from 6,004 (blue), 6,104 (black), and 6,204 m (red). (b) Pressure relative to the mean (dp) observed by the current meter at 6,208 m. Two times the mooring "jumped" approximately 1.2 m (~dbar) following a loss of three glass spheres. (c) Power (P) spectra as a function of frequency in cycles per day (cpd) of the red temperature series from 6,204 m, logarithm of 200 m vertically averaged dissipation rate (light blue; arbitrary scale), and vertical current inferred from temperature time series in panel (a) (green; arbitrary scale). The rooflike slopes σ^{-1}, σ^{+1} center at the w's peak frequency $\sim 0.5N = 0.95 f_h$ (small vertical dashed line).

The shorter-period variations in temperature are better visible in the spectral frequency (σ) domain (Fig. 3c; red). They show an energy hump between inertial frequency f and diurnal frequencies and a peak at the semidiurnal tidal frequency before progressively sharper rolling off with frequency between $2 f_h < \sigma < 6 f_h$ and eventually leveling off to white noise levels. From the temperature data, vertical motions are estimated associated with freely propagating internal waves, using the simple relationship $w_T = \partial \Theta / \partial t / (d\Theta/dz)_{200}$, implying an average value over the entire range of sensors as the vertical gradient is taken

over 200 m. At or near the tidal peak, the spectrum of w_T (Fig. 3c, green) "peaks" at $\sigma \approx 0.95 f_h \approx 0.5 N_{100}$ (in the following, the subscript 100 is dropped for large-scale N). On both sides of $0.5N$, its (nonpeak) spectral slope falls off at a rate of σ^{-1} for $0.5N < \sigma < 4 f_h$. This spectral sloping and spectral extent of the internal wave band are similar to previous acoustic Doppler current profiler w-spectra from the deep, weakly stratified Mediterranean Sea (van Haren and the ANTARES Collaboration 2014). The same slope is observed for $\log<[\varepsilon]>$ (Fig. 3c, light blue).

The vertical currents are directly associated with internal wave motions, as their spectral extent is largely between $f (\approx 0.33 f_h) \sim< \sigma \sim< N_m (\approx 4 f_h)$, the classic inertio-gravity frequency band, whereby the $N_m \approx 2N$, N_m denoting the root-mean-square (rms) local small-scale "thin-layer" buoyancy frequency here estimated over 2 m intervals ($N_{\max}$ denotes its maximum value). Over the period of a year, N and N_m are found to vary with time, associated with variations in turbulence parameter levels, but in general the internal wave band is about one decade wide in frequency here.

Computing turbulence parameters averaged over consecutive periods of 1 h (using a drift-correction window of 6 days), a time series of 200 m vertically averaged values is constructed in Figure 4. It is observed that with increasing midrange temperature (Fig. 4a), varying on the 20- to 40-day timescale besides tidal variations, stratification varies by up to a factor of 3 times the minimum value (Fig. 4b). The strong variation in rms turbulent displacements (Fig. 4c) and turbulence parameters (Fig. 4d and e), the latter over four orders of magnitude, are typical for ocean turbulence (e.g., Gregg 1989).

b. Detailed temperature observations

The detailed temperature sensor data reflect the dominance of the semidiurnal variations that are nearly in phase over the 200 m range (Fig. 5a). Vertical isotherm excursions are typically 50–100 m but can exceed the range of observations (e.g., on day 390 as discussed subsequently). During the relatively low-tidal-amplitude and the low-turbulence period of Figure 5, the associated 200 m vertically averaged turbulence dissipation rate shows a variation over three orders of magnitude only (Fig. 5b). It does not vary with a semidiurnal periodicity. Over the displayed 4 days, 200 m averaged values are as follows: $[<\varepsilon>] = 1.3 \pm 0.8 \times 10^{-11}$ m^2 s^{-3}, $[<K_z>] = 5 \pm 3 \times 10^{-5}$ m^2 s^{-1}, $[<N>] = 2.6 \pm 0.5 \times 10^{-4}$ s^{-1} = $1.9 \pm 0.4 f_h$.

A 1-day zoom of the temperature observations (Fig. 5c) demonstrates a strong asymmetry of the tidal motions, which are otherwise smooth showing few overturns that pass the threshold criterion (Fig. 5d). However, waters are not quiescent as may be inferred from the isotherm contours in Figure 5(c), which are drawn for the temperature depth-time distribution relative to the overall mean temperature (stratification) profile. In this contouring perspective, in the case of no mixing occurring, simple advection of cooler and warmer waters, with zero vertical phase lag, would show as vertical contour lines. In Figure 5(c), this is often the case, except for a few closed loops. In the same perspective of contouring
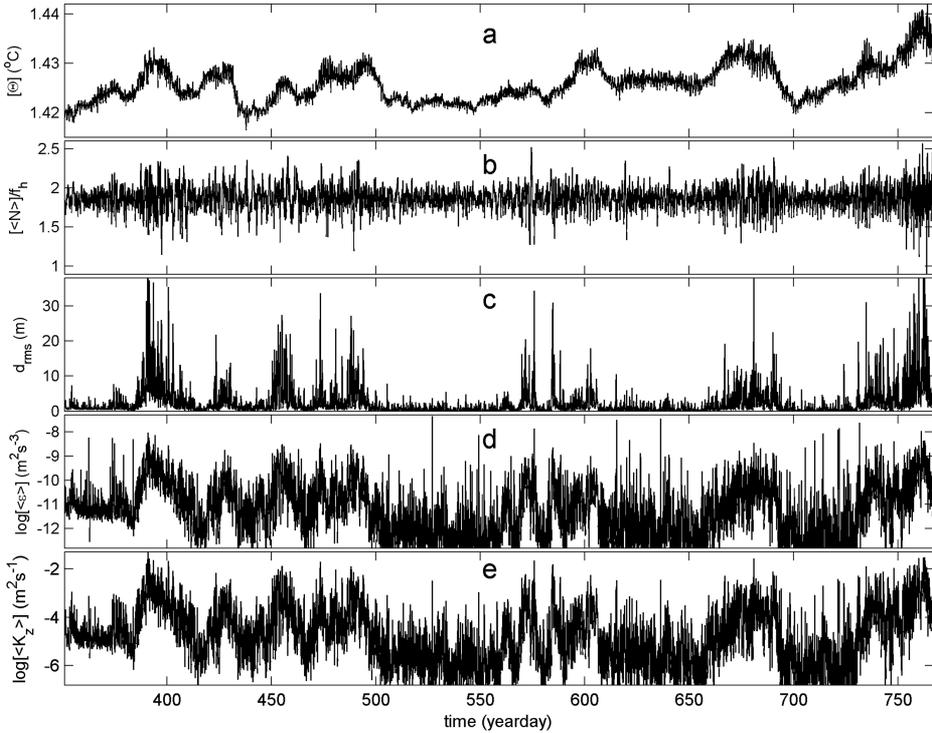
Figure 4. Entire time series of mainly turbulence characteristics over the range [6,004, 6,204] m, as inferred from 1 h averaged moored temperature sensor data. (a) Conservative temperature at 6,104 m. (b) Buoyancy frequency over the 200 m range, scaled with f_h. (c) Root-mean-square displacements over the 200 m range. (d) Vertically averaged dissipation rate. (e) Vertically averaged eddy diffusivity.

relative to the mean temperature (gradient) profile, homogeneous waters show as horizontal contours to the amount equivalent to the mean gradient but with a negative sign (so, totaling about seven contours over the 200 m range). An example will be given subsequently; it does not occur in Figure 5(c).

In addition to the few closed loops, the ragged nonsmooth appearance of the contours demonstrates, besides noise, small-scale turbulent activity. This may also be inferred from the continual variability of thin-layer stratification in Figure 5(e). Nonetheless, turbulence levels passing the noise threshold are low, but genuine turbulent overturning is observed as the duration of displacements never exceeds the 8 h mean buoyancy period in Figure 5(d).

High turbulence levels occur when inertial motions combine with tidal motions, while temperatures are (slowly) rising (see the example in Fig. 6). Over the displayed 4 days, 200 m averaged values are as follows: $[<\varepsilon>] = 1 \pm 0.6 \times 10^{-9}$ m^2 s^{-3}, $[<K_z>] = 4 \pm 2 \times 10^{-3}$ m^2 s^{-1}, $[<N>] = 2.5 \pm 0.5 \times 10^{-4}$ s$^{-1} = 1.8 \pm 0.4 f_h$, so that mean turbulence levels are
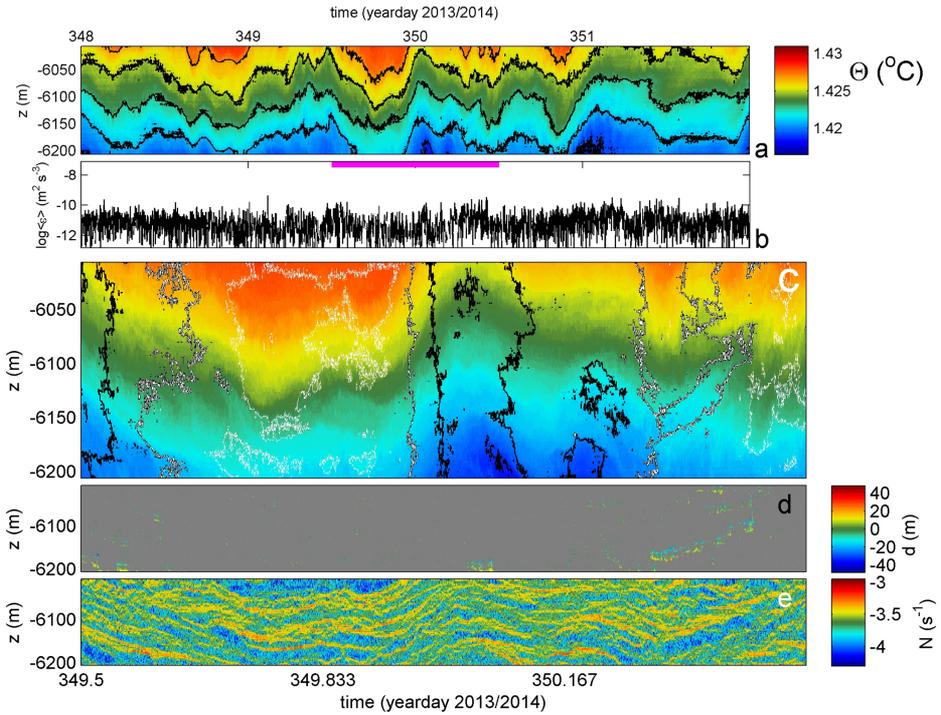
Figure 5. Example detail of high-resolution moored observations for a relatively weakly turbulent period from the beginning of the yearlong record, before the second loss of buoyancy glass spheres. (a) Four days of depth-time series of conservative temperature with black contours every 0.002°C. (b) Vertically averaged turbulence dissipation rate estimated from overturn displacements in the data in panel (a). (c) One-day depth-time temperature detail (time span corresponds to purple bar in panel b; same color scale as in panel a). Contours are drawn every 0.001°C delineating temperature difference with the overall mean temperature profile, after removing the temperature profile corresponding to $N = 1.9 f_h$. White contours indicate values exceeding the mean temperature profile, black & white mean temperature profile values, and black values below the mean temperature profile. About 1 min smoothing is applied for noise reduction. (d) Displacements from data in panel (c). (e) Buoyancy frequency for stably stratified reordered data of panel (c). The 200 m mean buoyancy frequency period is 8 ± 1 h, or the length between two x-axis tick marks.

about two orders of magnitude larger than for Figure 5. Besides the tidal period, the inertial period of 1.6 days is visible from day 389.4 onward. The amplitude exceeds the 200 m range of the sensors (e.g., around day 390). Although mean turbulence levels are relatively high, the variation with time of the 200 m mean dissipation rate exceeds five orders of magnitude including brief quiescent periods (Fig. 6b).

The number of contours in the detail image of Figure 6(c) is much larger than in Figure 5(c). During the higher turbulent period in Figure 6(c), closed loops are often seen, most
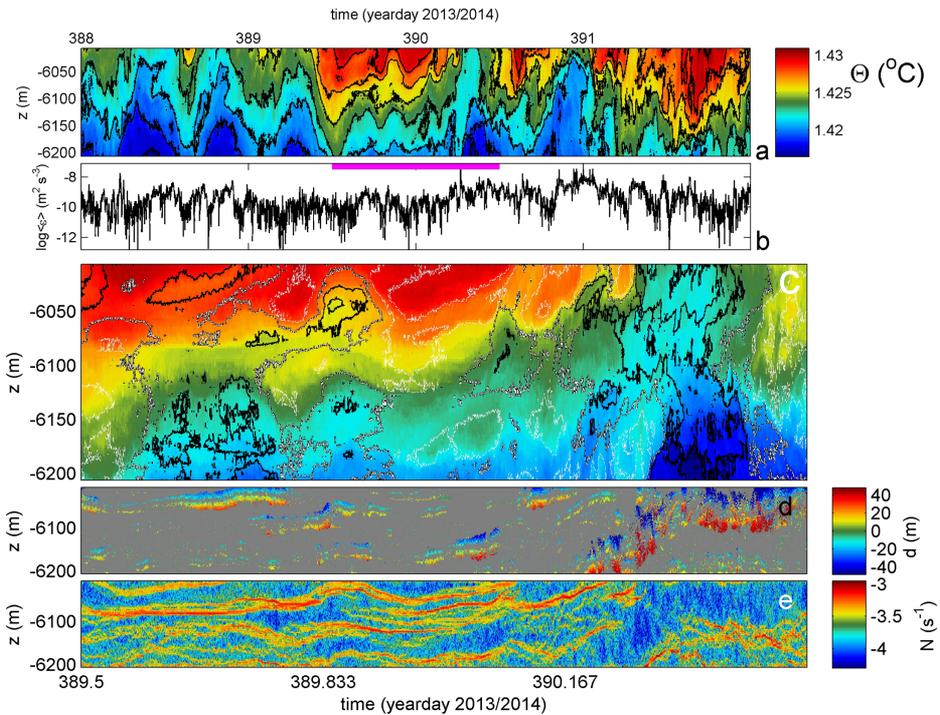
Figure 6. Same as in Figure 5, but for a relatively strongly turbulent period.

of them inclined (upward) in $[t, z]$-space. The period between days 390.25 (6,200 m) and 390.34 (6,000 m) shows the same incline, but in part of quasi-horizontally layered contours: in the lower half it is nearly homogeneous in conservative temperature as four contours are found over a range of 100 m, which nearly equals the mean stratification (that was removed for the contours). The upper half shows less layering (one to two contours), so that the overall remaining stratification equals f_h. The larger overturning is clearly demonstrated in the more frequent and larger displacements (Fig. 6d), compared with Figure 5(d).

The result is an intensified small-scale buoyancy frequency distribution (after reordering) in distinct layering with a doubling to approximately 50–100 m height of near-homogeneous layers (Fig. 6e), in comparison with Figure 5(e). As before, the duration, length in time, of the layers does not exceed the large-scale buoyancy period of 8 h, a third of the length of Figure 6(c)–(e).

4. Discussion and conclusions

It is hypothesized that the same shortness of duration (<8 h) of the thin well-stratified and near-homogeneous layers delineates the type of convection seen in the present observations.

As few Kelvin-Helmholtz billows have been observed, which would show as S shapes in stratification (N) images, shear instability is not expected to be the main initiator of convection, even though inertial motions do occur, which are known for their short vertical length scale thereby being important for shear in the ocean. As a result, (free) convection seems a more important candidate for the primary turbulent overturning. But, how can it be generated in stable stratification under the influence of internal waves?

Commonly, when a stably stratified (two-layer) fluid is under the influence of a body force, its vertical acceleration ($a = dw/dt$) should exceed that of gravity (g) for free convection to occur, no matter how weak the stratification (Sharp 1984; Dalziel 1993). However, motions in the ocean interior of quasi-continuously stratified fluid are not driven by a body force, but by an internal force of "reduced gravity," $g' = (g/\rho)\Delta\rho = N^2 L$, where the density difference is taken over a suitable vertical length scale, L. Intuitively, the physics may be described by a decomposition of motions into a mean (subinertial) field, a large-scale (tidal and inertial) internal wave field, and a small-scale (near the buoyancy frequency) internal wave field. However, the mathematical solution of the underlying dynamical equations is very complex (Krauss 1966) and still has to be done.

Hypothesizing, we estimate accelerations for the present weakly stratified conditions. For the given mean buoyancy frequency $N = 2.6 \times 10^{-4}$ s^{-1}, we find an internal wave acceleration of $a = Nw = 2 \times 10^{-6}$ m s^{-2} for w estimated from temperature observations. The condition $a > g'$ implies $L < 40$ m. Thus, for realistic internal waves, accelerations can be sufficient to create free convection, provided low-frequency inertial-tidal internal waves interact with waves near the buoyancy frequency to create sufficiently strong vertical and nonlinear motions.

After initiation and a particular lapse of time ($\sim 1/f = 6$ h here), such convection will spread "slant-wise" in the direction of the Earth rotational vector in near-homogeneous waters, as shown in laboratory experiments of (Sheremet 2004). When the Earth rotational and gravity vectors are at a particular angle, which is the case when observations are not made at the North Pole, such "slanted" convection results in weak, but nonhomogeneous stratification (when measured in the direction of gravity, as is common in the ocean). Thus, they become limited by the overall mean stratification as in stratified shear flows, and for which a limiting duration of 0.95 times the large-scale buoyancy period has been observed (van Haren and Gostiaux 2015). The presently observed overturning over timescales shorter than the buoyancy period is most probably genuine stratified turbulence, as salinity-compensated intrusions, if present, have durations also exceeding the buoyancy period.

It remains to be investigated how precisely the interaction plays between tidal and inertial motions (and perhaps subinertial motions). Besides the collapse of horizontal density gradients ("fronts"), inertial waves may be generated from Taylor columns induced by inertial (tidal) waves. Davidson (2013) suggests two conditions for the latter inertial wave generation via turbulence from (internal wave) vorticity transfer. One condition reads that the Reynolds number should be large, Re $= ul/\nu >> 1$, with ν the kinematic viscosity and u and l suitable velocity and length scales, respectively. The other condition requires the

Rossby number to become of order unity Ro $= u/\Omega l \approx 1$, after being much larger initially. The first condition is easily met here, as Re $\sim O(10^6)$. The second condition is met if we take for length scale the vertical scale $l_z = 50 - 100$ m of homogeneous layers, which we assume points along the direction of the Earth rotational vector, $l = l_z/\sin \varphi = 150 - 300$ m, when $u = 0.01 - 0.02$ m s^{-1}. Such low current values were measured. The associated tidal and inertial vertical motions have typical amplitudes of 0.01 m s^{-1}.

The combination of tidal and inertial motions is partially imperative for the observed turbulence generation. Tidal motions have large vertical scales, with little vertical phase variation (over the 200 m range of observations). This implies very weak shear. Large shear is mainly associated with the near-inertial motions. The latter thus have shorter vertical length scales, which may add to the tilting of isopycnals, as observed in Figure 6(c). It seems that this leads to oblique nonlinear motions, which results in strong convection. Although the precise interactions cannot be established from the single mooring data, it is not unlikely that the enhanced near-inertial motions are associated with the periodic (20–50 days) arrival of warmer waters. The present observations are too limited to determine the source of these waters, but the periodicity of variation points to mesoscale eddy activity, probably at the interface between Caribbean and North Atlantic waters. The result of these interactions is a vertical convection that replenishes the (top of the) PRT waters with fresh materials. It stresses the importance of internal wave motions for mixing and vertical exchange for redistribution of suspended materials and life, also in such deep parts of the ocean.

REFERENCES

Dalziel, S. B. 1993. Rayleigh-Taylor instability: Experiments with image analysis. Dyn. Atmos. Oceans, *20*(1–2), 127–153. doi: 10.1016/0377-0265(93)90051-8

Davidson, P. A. 2013. Turbulence in Rotating, Stratified and Electrically Conducting Fluids. Cambridge: Cambridge University Press, 681 pp.

Dillon, T. M. 1982. Vertical overturns: A comparison of Thorpe and Ozmidov length scales. J. Geophys. Res.: Oceans, *87*(C12), 9601–9613. doi: 10.1029/JC087iC12p09601

Gargett, A. E. 1984. Vertical eddy diffusivity in the ocean interior. J. Mar. Res., *42*(2), 359–393. doi: 10.1357/002224084788502756

Geyer, W. R., and J. D. Smith. 1987. Shear instability in a highly stratified estuary. J. Phys. Oceanogr., *17*(10), 1668–1679. doi: 10.1175/1520-0485(1987)017%3C1668:SIIAHS%3E2.0.CO;2

Gregg, M. C. 1989. Scaling turbulent dissipation in the thermocline. J. Geophys. Res.: Oceans, *94*(C7), 9686–9698. doi: 10.1029/JC094iC07p09686

Intergovernmental Oceanographic Commission (IOC), Scientific Committee on Oceanic Research, and International Association for the Physical Sciences of the Oceans. 2010. The International Thermodynamic Equation of Seawater – 2010: Calculation and Use of Thermodynamic Properties. IOC, Manuals and Guides No. 56. Paris: UNESCO, 196 pp.

Krauss, W. 1966. Methoden und Ergebnisse der theoretischen Ozeanographie, Vol. II, Interne Wellen. Berlin: Borntraeger, 248 pp.

Levine, M. D., and T. J. Boyd. 2006. Tidally forced internal waves and overturns observed on slope: Results from HOME. J. Phys. Oceanogr., *36*(6), 1184–1201. doi: 10.1175/JPO2887.1

Moum, J. N., D. R. Caldwell, and C. A. Paulson. 1989. Mixing in the equatorial surface layer and thermocline. J. Geophys. Res.: Oceans, *94*(C2), 2005–2021. doi: 10.1029/JC094iC02p02005

Oakey, N. S. 1982. Determination of the rate of dissipation of turbulent energy from simultaneous temperature and velocity shear microstructure measurements. J. Phys. Oceanogr., *12*(3), 256–271. doi: 10.1175/1520-0485(1982)012<0256:DOTROD>2.0.CO;2

Osborn, T. R. 1980. Estimates of the local rate of vertical diffusion from dissipation measurements. J. Phys. Oceanogr., *10*(1), 83–89. doi: 10.1175/1520-0485(1980)010<0083:EOTLRO>2.0.CO;2

Seim, H. E., and M. C. Gregg. 1994. Detailed observations of a naturally occurring shear instability. J. Geophys. Res.: Oceans, *99*(C5), 10049–10073. doi: 10.1029/94JC00168

Sharp, D. H. 1984. An overview of Rayleigh-Taylor instability. Phys. D, *12*(1–3), 3–18. doi: 10.1016/0167-2789(84)90510-4

Sheremet, V. A. 2004. Laboratory experiments with tilted convective plumes on a centrifuge: A finite angle between the buoyancy and the axis of rotation. J. Fluid Mech., *506*, 217–244. doi: 10.1017/S0022112004008572

Smith, W. H. F., and D. T. Sandwell. 1997. Global sea floor topography from satellite altimetry and ship depth soundings. Science, *277*(5334), 1957–1962. doi: 10.1126/science.277.5334.1956

Thorpe, S. A. 1977. Turbulence and mixing in a Scottish loch. Philos. Trans. R. Soc., A, *286*(1334), 125–181. doi: 10.1098/rsta.1977.0112

van Haren, H. 2008. Abrupt transitions between gyroscopic and internal gravity waves: The mid-latitude case. J. Fluid Mech., *598*, 67–80. doi: 10.1017/S0022112007009524

van Haren H, and L. Gostiaux. 2012. Detailed internal wave mixing observed above a deep-ocean slope. J. Mar. Res., *70*(1), 173–197. doi: 10.1357/002224012800502363

van Haren, H., and L. Gostiaux. 2015. Distinguishing turbulent overturns in high-sampling-rate moored thermistor string observations. J. Mar. Res., *73*(1–2), 17–32. doi: 10.1357/002224015815782661

van Haren, H., M. Laan, D.-J. Buijsman, L. Gostiaux, M. G. Smit, and E. Keijzer. 2009. NIOZ3: Independent temperature sensors sampling yearlong data at a rate of 1 Hz. IEEE J. Oceanic Eng., *34*(3), 315–322. doi: 10.1109/JOE.2009.2021237

van Haren, H., and C. Millot. 2006. Determination of buoyancy frequency in weakly stable waters. J. Geophys. Res.: Oceans, *111*, C03014. doi: 10.1029/2005JC003065

van Haren, H., and the ANTARES Collaboration. 2014. High-frequency internal wave motions at the ANTARES site in the deep western Mediterranean. Ocean Dyn., *64*(4), 507–517. doi: 10.1007/s10236-014-0702-0